

The Mechanism of Oxide Ion Conductivity in Bismuth Rhenium Oxide, $\text{Bi}_{28}\text{Re}_2\text{O}_{49}$

Julia L. Payne¹, James D. Farrell¹, Alistair M. Linsell¹, Mark R. Johnson² and Ivana Radosavljević Evans^{1,*}

¹ Department of Chemistry, Durham University, Science Site, Durham DH 1 3LE, U.K.

² Institut Laue Langevin, Grenoble, F-38042, France

* E-mail: ivana.radosavljevic@durham.ac.uk

Abstract

We have carried out a combined experimental and computational study of oxide ion conductor $\text{Bi}_{28}\text{Re}_2\text{O}_{49}$, with the aim of elucidating the conductivity mechanisms and pathways in this material. Single crystals of $\text{Bi}_{28}\text{Re}_2\text{O}_{49}$ were grown from melt and the structure investigated for the first time by single crystal X-ray diffraction. The structural model obtained is consistent with the Re atoms in $\text{Bi}_{28}\text{Re}_2\text{O}_{49}$ being both four- and six-coordinate, in a 3:1 ratio, in agreement with previous EXAFS and IR spectroscopy studies. The thermal displacement parameters of the oxygen atoms bonded to Re suggest substantial disorder of the Re coordination polyhedra. *Ab-initio* molecular dynamics simulations were performed to probe the oxide ion migration pathways in $\text{Bi}_{28}\text{Re}_2\text{O}_{49}$ and the roles of the Bi-O and Re-O sublattices. The key conclusion is that the ability of Re to support variable coordination environments is vitally important in $\text{Bi}_{28}\text{Re}_2\text{O}_{49}$; it provides a mechanism for ‘self-doping’ of the structure, i.e. the creation of O^{2-} vacancies in the fluorite-like Bi-O sublattice by exchange of O atoms with the Re-O sublattice, and the subsequent increase of the average coordination number of Re. All three crystallographically unique oxygen sites in the Bi-O sublattice play roles in the ionic migration processes, by facilitating the O^{2-} exchange between the ReO_x groups and by contributing to the O^{2-} diffusion *via* the vacancy-hopping mechanisms.

1. Introduction

Oxide ion conductors have applications in devices such as solid oxide fuel cells, oxygen pumps and oxygen separation membranes.[1-3] High operating temperatures are a limiting factor in some applications, hence much research has centred on materials which exhibit high oxide ion conductivity at low and intermediate temperatures (400–600°C). Although many

different structural families of oxide ion conductors exist, fluorite-related materials remain one of the best studied. The high conductivity exhibited by δ -Bi₂O₃ ($\sim 1 \text{ S cm}^{-1}$ at 750 °C), which possesses the fluorite structure with 25% of anion sites vacant and disordered, has led to the study of many doped Bi₂O₃-related oxide ion conductors. The cubic structures with the unit cell parameter $a \sim 5.5 \text{ \AA}$ and space group Fm-3m may be retained by low-level doping of Bi₂O₃ with different cations [4-7] (including Er³⁺, Y³⁺, V⁵⁺, Mo⁵⁺, W⁶⁺, Nb⁵⁺ and Ta⁵⁺), although the stability of these materials can be an issue.[8]

An in-depth understanding of the ionic mobility mechanisms is necessary for the successful discovery and preparation of new oxide ion conductors which will overcome the limitations of the currently used materials. Extensive experimental and computational work has led to the proposal of several general classes of mechanism for oxide ion migration: the vacancy mechanism; the interstitial and interstitialcy mechanisms; the cooperative mechanism and the variable coordination number mechanism.[9-11] The mechanism occurring in fluorite-related oxide ion conductors has been thought to proceed principally *via* vacancies, whilst some apatites and melilite-related compounds exhibit an interstitial mechanism.[9, 12] La_{1-x}Ba_{1+x}GaO_{4-x/2} related oxide ion conductors exhibit a cooperative mechanism which requires exchange of oxygen between GaO₄ groups, forming Ga₂O₇ units as intermediates in the conduction process.[10] The crystal structure of α -La₂Mo₂O₉ was found to contain Mo in three different types of coordination environments (4-, 5- and 6-coordinate) and to undergo an order-disorder phase transition to the highly conducting β -La₂Mo₂O₉ polymorph.[11] Based on this structural work, it was proposed that the ability of cations to support variable coordination environments was important for the oxide ion migration pathways.[11]

The structure of Bi₂₈Re₂O₄₉ was first determined by Crumpton *et al.* using powder neutron diffraction.[13] Bi₂₈Re₂O₄₉ has unit cell parameters $a = 8.7216(1) \text{ \AA}$ and $c = 17.4177(2) \text{ \AA}$ and crystallises in tetragonal space group $I4/m$. It consists of isolated rhenium oxide polyhedra (located at the body centre and corners of the unit cell) in a fluorite-type matrix. EXAFS and IR spectroscopy suggested that 75% of the Re atoms were present as ReO₄⁻ tetrahedra and the remaining 25% as ReO₆⁵⁻ octahedra. However, the oxygen atoms bonded to Re could not be located from the neutron diffraction data and the structure refinement was carried out by assuming that only ReO₄⁻ tetrahedra were present. The ionic conductivity of Bi₂₈Re₂O₄₉ and subsequently the conductivities of the related Bi₂₅Ln₃Re₂O₄₉ ($Ln = \text{La, Pr}$) compounds have been reported in the literature.[13, 14] The substituted compounds were found to readily convert from the metastable cubic to tetragonal structures, with a significant

drop in conductivity ($2.3 \times 10^{-3} \text{ S cm}^{-1}$ at 500°C was found for $\text{Bi}_{28}\text{Re}_2\text{O}_{49}$ vs. $2.8 \times 10^{-4} \text{ S cm}^{-1}$ and $2.1 \times 10^{-4} \text{ S cm}^{-1}$ for $\text{Bi}_{25}\text{La}_3\text{Re}_2\text{O}_{49}$ and $\text{Bi}_{25}\text{Pr}_3\text{Re}_2\text{O}_{49}$, respectively). From powder neutron diffraction, the *Ln* substituents were found to occupy only one of the three unique Bi sites – Bi3, bonded to the oxygen site O3 adjacent to the layers containing Re atoms. It was therefore proposed that that the O3 site plays an important role in the conduction mechanism by providing a pathway for oxygen exchange between the Re centres.[14]

The aims of this work were to investigate the structure and the oxide ion migration mechanism in the fluorite-related $\text{Bi}_{28}\text{Re}_2\text{O}_{49}$. Although the length- and time-scales of *ab-initio* molecular dynamics (AIMD) simulations are invariably too short to provide reliable ensemble averages, such as diffusion rates, they are long enough to reveal diffusion mechanisms, provided care is taken to prepare realistic starting structures. We have previously used AIMD simulations to probe the oxide ion pathways in the fluorite-based $\text{Bi}_{10}\text{La}_8\text{O}_{27}$, where we found the vacancy mechanism to dominate.[15] In this work, the particular goal of the AIMD simulations was to determine the role of the variable coordination of the Re atoms in the conduction process and the types of interaction between the Bi-O and the Re-O sublattices.

2. Experimental

Single crystal growth and X-ray diffraction

A polycrystalline sample of $\text{Bi}_{28}\text{Re}_2\text{O}_{49}$ was prepared by intimately mixing stoichiometric quantities of Bi_2O_3 and NH_4ReO_4 and firing the mixture at 800°C for 48 hours. Single crystals were grown by melting a small amount of $\text{Bi}_{28}\text{Re}_2\text{O}_{49}$ at 900°C , slow-cooling to 400°C at $1.2^\circ\text{C}/\text{hour}$ and to room temperature at $10^\circ\text{C}/\text{hour}$. A prism-shaped yellow crystal measuring $0.02 \times 0.06 \times 0.08 \text{ mm}^3$ was selected for data collection. X-ray diffraction data were collected at 120 K on a Bruker SMART 6000 three-circle diffractometer with a CCD detector, using Mo $K\alpha$ radiation. A full sphere of data was recorded, with a counting time of 40 seconds per frame. A multiscan absorption correction was applied to the raw data and the resulting R_{int} was 6.7%. Frames were integrated using the program SAINT+ and data reduction carried out using XPREP. [16] The crystal structure was solved by a combination of direct methods, used to locate the metal sites, and difference Fourier maps that revealed the oxygen atom positions, using SIR92 and Crystals software.[17][18] The final structure refinement was carried out in Topas Academic ($R_{\text{int}}=6.1\%$), with all atomic displacement parameters treated anisotropically, except the split Re site (*vide infra*). [19]

***Ab-initio* molecular dynamics simulations**

Simulations were carried out using Vienna *ab-initio* simulation package (VASP).[20, 21] DFT-based first principle calculations were performed using the projector augmented wave (PAW)[22] formalism of the Kohn-Sham DFT[23, 24] at the generalised gradient approximation level (GGA). The GGA was formulated by the Perdew-Burke-Ernzerhof (PBE)[25, 26] density functional. The Gaussian broadening technique was adopted and all results were well converged with respect to k -mesh and energy cut-off for the plane wave expansion. AIMD simulations were performed in the NVT ensemble, temperature being controlled with a Nosé thermostat. Simulations were carried out at four temperatures (773 K, 973 K, 1173 K and 1373 K), using geometry optimised structures in the $1 \times 1 \times 2$ supercell as starting models. A time step of 2 fs was used and simulations were ran for 20 000 steps, giving 40 ps trajectories. Trajectory visualisation was carried out using LAMP[27] and the coordination numbers and mean-square displacements (MSDs) were determined using nMOLDYN.[28]

3. Results and Discussion

Since the $\text{Bi}_{28}\text{Re}_2\text{O}_{49}$ structure has already been reported from powder diffraction data [14], we briefly describe only the improvements of the structural model based on our single crystal diffraction data analysis (Table 1), as well as the key structural features needed for the interpretation of the simulations. Re atoms are located on the four-fold axis and the shortest distance between two Re centres corresponds to the length of the a -axis (8.7 Å, Figure 1a). Three unique O sites (O1-O3) were found bonded to Bi atoms and forming OBi_4 tetrahedra. In contrast with the previous structural work in which the oxygen atoms bonded to Re could not be located and the refinement was carried out by assuming that only ReO_4^- tetrahedra were present (leading to the overall stoichiometry $\text{Bi}_{28}\text{Re}_2\text{O}_{48}$), in our single crystal work two further unique O sites (O4 and O5), arranged in an octahedral geometry around Re, were readily located from the difference Fourier maps. These are partially occupied (*vide infra*), giving a range of possible Re coordination environments; the Re coordination polyhedra will therefore be referred to as the ReO_x groups. The nearest-neighbour ReO_x groups are separated by fluorite-like Bi-O sublattice formed by corner- and edge-sharing OBi_4 tetrahedra.

Table 1: Atomic fractional coordinates and site fractional occupancies for $\text{Bi}_{28}\text{Re}_2\text{O}_{49}$

Site	x	y	z	Site	Occ
Bi1	0.70058(9)	0.89430(8)	0.67043(4)	16i	1
Bi2	0.78806(12)	0.55405(12)	0.50000	8h	1
Bi3	0.50000	0.50000	0.65539(8)	4e	1
Re1	1.00000	1.00000	0.48569(19)	4e	0.5
O1	0.50000	1.00000	0.6233(12)	8g	1
O2	0.5757(16)	0.7528(15)	0.74385(91)	16i	1
O3	0.6304(17)	0.6785(16)	0.57739(88)	16i	1
O4	1.00000	1.00000	0.6155(34)	4e	0.75
O5	1.0008(85)	1.2101(58)	0.50000	8h	0.75

$a = 8.7216(1) \text{ \AA}$, $c = 17.4177(2) \text{ \AA}$, space group $I4/m$

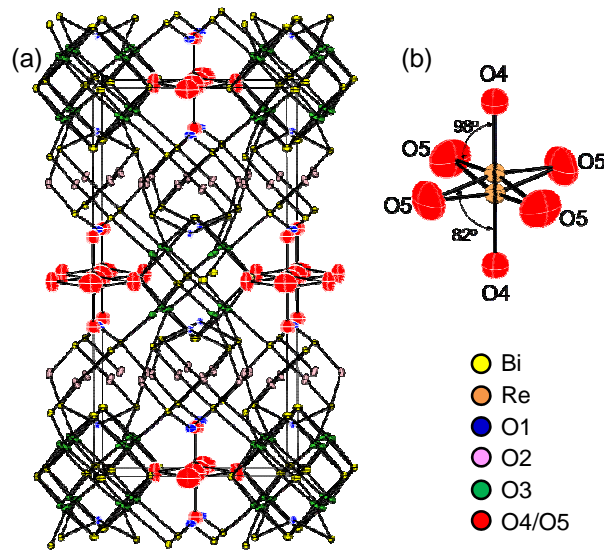


Figure 1. (a) View of the $\text{Bi}_{28}\text{Re}_2\text{O}_{49}$ structure down the b-axis, with atomic displacement parameters plotted at 50% probability. (b) Coordination environment around Re atom displaced off the mirror plane perpendicular to the c-axis. The size and shape of the O4 and O5 thermal parameters suggest likely disorder of the ReO_x coordination polyhedra.

The Re coordination environment is highly-distorted octahedral (Figure 1b). Re is displaced off the mirror plane perpendicular to the c-axis by 0.25 \AA , and its coordination sphere comprises oxygen sites O4 (axial positions) and O5 (equatorial positions). The Re-O bond lengths range from $1.76(6) \text{ \AA}$ to $2.26(6) \text{ \AA}$, and the O-Re-O angles deviate up to 8° from the ideal 90° angles. A structural model with all five unique oxygen sites fully occupied leads to

composition $\text{Bi}_{28}\text{Re}_2\text{O}_{52}$ and early refinement cycles in which all atomic displacement parameters were treated as isotropic suggested that oxygen sites O1-O3 (belonging to the Bi-O sublattice) were fully occupied, while O4 and O5 were partially occupied. Simulated annealing was used to refine fractional occupancies of these two sites, while keeping their isotropic temperature factors fixed at 0.05 \AA^2 and restraining the overall oxygen content. This gave values of 0.73(8) and 0.78(6) for O4 and O5, respectively, i.e. both sites appear $\frac{3}{4}$ occupied, within a standard uncertainty. In subsequent stages of refinement, the fractional occupancies of these sites were therefore fixed at 0.75. This corresponds to the nominal $\text{Bi}_{28}\text{Re}_2\text{O}_{49}$ composition and to an average Re coordination number of 4.5. Our single crystal X-ray diffraction analysis is therefore consistent with the observation of Crumpton *et al.* [13], based on IR spectroscopy and EXAFS, that the structure contains tetrahedral and octahedral Re atoms in a 3:1 ratio.

Ab-initio molecular dynamics simulations were carried out in order to determine the roles of the Bi-O sublattice and the ReO_x structural motifs in oxide ion migration. The simulations were performed at four temperatures (773 K, 973 K, 1173 K and 1373 K). The basic model for simulations was derived by transforming the experimental structure into space group P1, setting all crystallographic sites to be fully occupied and randomly removing the excess oxygen sites to obtain the correct stoichiometry. The $1 \times 1 \times 2$ supercell used corresponds to a total of 158 atoms in the simulation box ($\text{Bi}_{56}\text{Re}_4\text{O}_{98}$), with a 3:1 ratio of 4- and 6-coordinate Re atoms. This model is in agreement both with the stoichiometry of the compound and the average structure obtained by diffraction. Geometry optimisation was carried out before the molecular dynamics simulations.

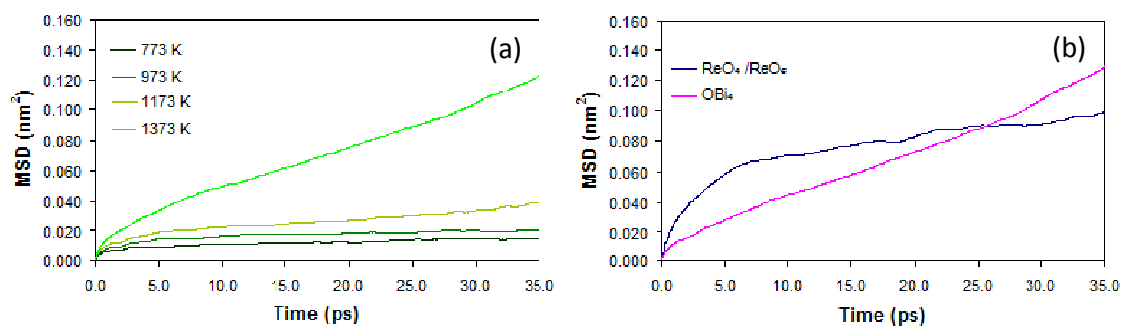


Figure 2. (a) The MSDs of oxide ions over the course of the simulations at four temperatures (773 K, 973 K, 1173 K and 1373 K). (b) The MSDs of the oxygen atoms originating from the Re-O and the Bi-O sublattices in the initial geometry optimised model, during the course of the simulation at 1373 K in the $1 \times 1 \times 2$ supercell.

Mean-square displacements (MSDs) of oxide ions were calculated to compare the mobility at different temperatures and to distinguish between vibrational and diffusional motion. Observation of a linearly increasing MSD signifies diffusion, whilst plateaus signify vibrational or rotational motion. The MSD plots obtained in the simulations are shown in Figure 2. As expected, the MSDs increase with increasing temperature, with the shape of the curves changing from essentially a plateau at 773 K to a linearly increasing curve at 1373 K, indicating the change from primarily vibrational/rotational to diffusional motion at the highest temperature simulated (Figure 2a). Figure 2b shows the MSDs at 1373 K of the oxygen atoms initially belonging to the Bi-O and Re-O sublattices. This analysis reveals qualitatively different behaviour for these oxygen atoms: those originating from the Bi-O sublattice clearly show translational diffusion, whereas those from the Re-O sublattice mainly undergo rotational diffusion in a sphere of diameter $\sim 2.5 \text{ \AA}$.

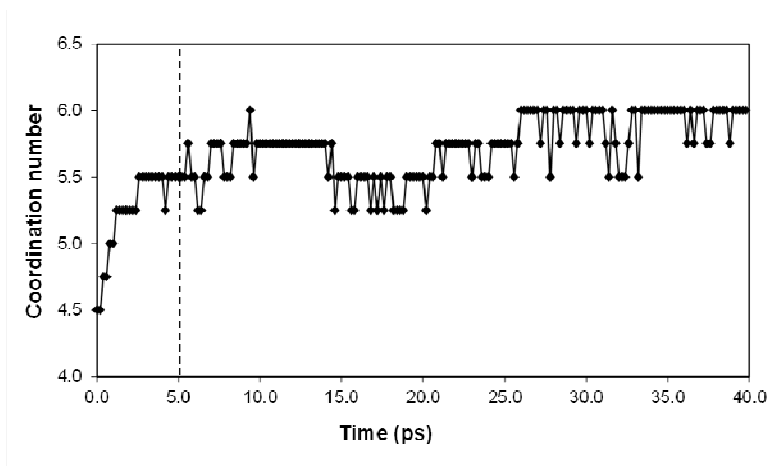


Figure 3. Evolution of the Re average coordination number over the course of the AIMD simulations at 1373 K. The dashed line separates the equilibration (0–5 ps) and the production (5–40 ps) phases of the simulation.

The variation of the average Re coordination number during the 1373 K simulations calculated using the bond length range observed in the single crystal structure determination, is shown in Figure 3. The most significant observation is that during the equilibration phase (0–5 ps) the average Re coordination number quickly increases from the initial value of 4.5, and this value is not reached again during the production phase of the simulation. Re atoms remain essentially 5- or 6-coordinate, with the average coordination numbers of 5.67 over the course of the simulation.

The typical mechanism by which the increase of the Re coordination number occurs has clear implications for the oxide ion conduction pathways in $\text{Bi}_{28}\text{Re}_2\text{O}_{49}$, as illustrated in

Figures 4a-e, which depict the same structural fragment at five points in the trajectory (at 0, 8.8, 9.0, 10.6 and 11.4 ps).

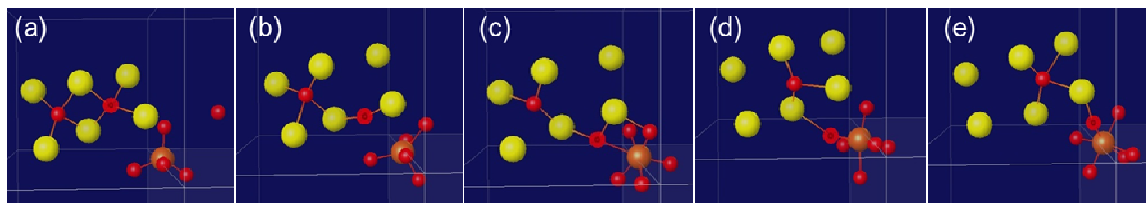


Figure 4: Oxygen exchange between the Bi-O and the Re-O sublattices in $\text{Bi}_{28}\text{Re}_2\text{O}_{49}$. (a) Initial configuration consisting of a pair of edge-shared OBi_4 tetrahedra and an adjacent ReO_4 ; an O atom belonging to a different OBi_4 group (omitted for clarity) is on the right-hand side. (b) Transient state formed by the O atom which has left its site, is diffusing through the edge of its OBi_4 group; the second adjacent O atom has entered the Re coordination sphere, giving rise to a ReO_5 square pyramid. (c) The first O atom transfer is completed and Re is six-coordinate ReO_6 . (d) The second O atom from the original fluorite-type block diffuses into the adjacent vacancy. (e) The vacancy hop is completed and a new $\square\text{Bi}_4$ vacancy is left behind. Red spheres represent O atoms, orange spheres are Re atoms and yellow spheres are Bi atoms.

Figure 4a shows the initial structural fragment containing two edge-shared OBi_4 tetrahedra in proximity of a ReO_4 tetrahedron; the O atom on the right-hand side of the picture belongs to another adjacent Bi-O fragment, which has been omitted for clarity. By 9.0 ps (Figure 4c), an oxygen from the fluorite-type block has diffused through the edge of its OBi_4 group into the Re coordination sphere, leaving behind a $\square\text{Bi}_4$ unit (\square = vacancy), i.e. creating a vacancy in the Bi-O sublattice; the O atom from the other Bi-O fragment has undergone similar diffusion, creating a ReO_6 distorted octahedron. The second O atom from the original Bi-O fragment has already started moving into the neighbouring $\square\text{Bi}_4$ vacancy; by 11.4 ps, it has adopted a four-fold OBi_4 coordination in the new position, and left behind another vacancy (Figure 4e). The diffusion process in the Bi-O sublattice can continue by mechanisms typical of stabilised $\delta\text{-Bi}_2\text{O}_3$ phases, i.e. by hopping between two neighbouring OBi_4 tetrahedra through the shared edge (Figure 5a), or indirectly via the intervening octahedral $\square\text{Bi}_6$ vacant sites (Figure 5b).

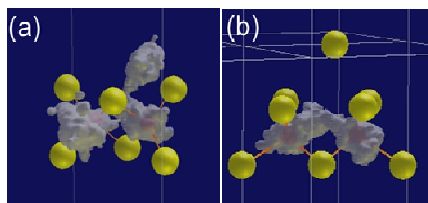


Figure 5. Mechanisms of oxide ion migration through the Bi-O sublattice in $\text{Bi}_{28}\text{Re}_2\text{O}_{49}$. White displacement clouds represent volumes visited by O^{2-} ions. (a) Oxygen diffusion between two neighbouring OBi_4 tetrahedra through a shared edge. (b) Oxygen diffusion through the face of an OBi_4 tetrahedron into an intervening $\square\text{Bi}_6$ octahedral vacancy and onwards into the next $\square\text{Bi}_4$ tetrahedron.

This represents a typical mechanism, which was observed repeatedly in the simulations at 1373K. In essence, the increase of the average coordination number of Re from the initial value of 4.5 can be viewed as 'self-doping' of the structure, by analogy with vacancy generation by chemical aliovalent doping of parent fluorite-type structures, which enables long-range O^{2-} conductivity by vacancy-hopping mechanisms facilitated by the high polarisability of the Bi-O sublattice.

Our findings from the AIMD simulations display certain similarities with the experimentally-based conclusions of Holmes *et al.*, who used ^{17}O solid state NMR to provide detailed insight into the conductivity mechanism in $\delta\text{-Bi}_2\text{O}_3$ related columnar phase $\text{Bi}_{26}\text{Mo}_{10}\text{O}_{69}$, which had previously been the subject of much debate based on structural work alone.[29] At low temperatures, the exchange of oxygen atoms between the MoO_4^{2-} tetrahedra *via* a partially occupied oxygen site was observed. At higher temperatures, resonances from the MoO_4^{2-} tetrahedra and the $[\text{Bi}_{12}\text{O}_{14}]_{\infty}$ columns started to coalesce, indicating that oxygen exchange between the Bi-O and the Mo-O sublattices was occurring. Importantly, no evidence of oxygen exchange within the $[\text{Bi}_{12}\text{O}_{14}]_{\infty}$ columns was observed before the onset of the Bi-O/Mo-O exchange.[29] This is similar to the results of our AIMD simulations on $\text{Bi}_{28}\text{Re}_2\text{O}_{49}$, which suggest that the 'self-doping' of the structure by oxygen extraction from the Bi-O into the Re-O sublattice must occur first in order for the long-range O^{2-} conduction to proceed. The mechanism by which this is seen to occur in our simulations, namely the increase of the average coordination number of Re, is consistent with the known crystal chemistry of the Re^{7+} cation, which can exist in four-, five- and six-fold coordination environments. [30]

The final issue we addressed by the AIMD simulations was the role of the three crystallographically unique oxygen sites within the Bi-O sublattice (labelled O1, O2 and O3

in the crystal structure, Figure 1) in the conduction process. As seen in Figure 6a, in which white displacement clouds represent volumes visited by the O^{2-} ions, the role of the O3 oxygens is to provide a pathway for the exchange of oxide ions between adjacent ReO_x polyhedra (Figure 6a), by mechanisms depicted in detail in Figure 4.

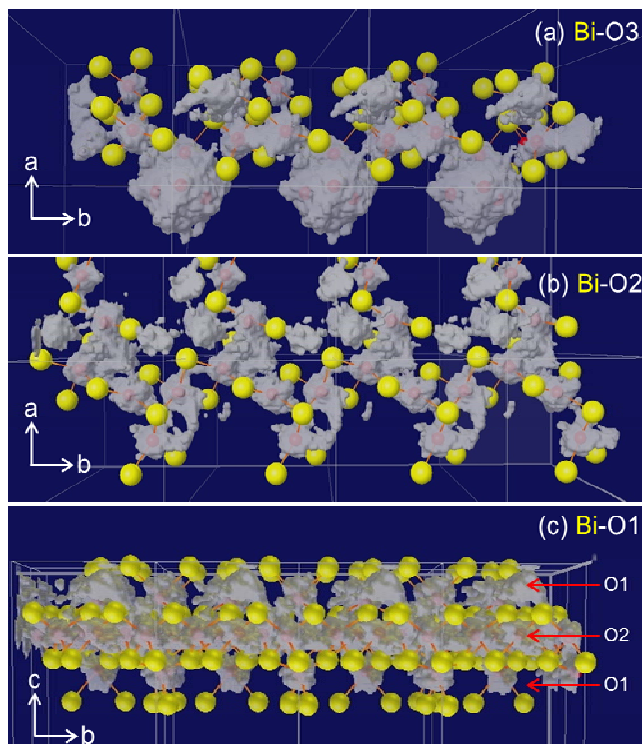


Figure 6. Roles of the three crystallographic O atom sites in the Bi-O sublattice in $Bi_{28}Re_2O_{49}$. White clouds represent volumes visited by O^{2-} ions. (a) O3 sites facilitate the exchange of O^{2-} ions between adjacent ReO_x polyhedra; (b) O2 sites provide a pathway for vacancy-hopping in the (ab) plane; (c) O1 sites contribute through O^{2-} exchange with the O2 layers.

Our computational results thus fully support the prediction regarding the importance of the O3 site, made by Hervoches *et al.*[14] based on their neutron diffraction work. In addition, simulations reveal that the O2 and O1 sites also participate in the conduction process. Figure 6b shows a small part of the Bi-O sublattice formed by corner- and edge-sharing O_2Bi_4 tetrahedra; the inter-connected oxygen displacement clouds suggest that the O2 sites provide pathways for O^{2-} migration in layers perpendicular to the c -axis, by vacancy-hopping

mechanisms typical of fluorite-type structures. Finally, the O1 sites appear to play an auxiliary role by facilitating the oxide ion exchange with the O2 layers “sandwiched” between them, i.e. along the c -axis (Figure 6c).

It is also worth pointing out that a recent variable temperature neutron diffraction study of a structurally related rhenate oxide ion conductor, Bi_3ReO_8 , suggests that variable Re coordination plays a role in the behaviour of this material, as well. With increasing temperature, accumulation of nuclear density in the vicinity of ReO_4 tetrahedra was observed in difference Fourier maps, in positions consistent with the formation of ReO_5 groups. [31]

4. Conclusions

Single crystals of oxide ion conductor $\text{Bi}_{28}\text{Re}_2\text{O}_{49}$ were grown from melt and the structure of the material was investigated by single crystal X-ray diffraction. The average structure is consistent with the Re atoms in $\text{Bi}_{28}\text{Re}_2\text{O}_{49}$ being both four- and six-coordinate, in a 3:1 ratio, in agreement with previous EXAFS and IR spectroscopy studies. The size and shape of the thermal displacement parameters obtained for the oxygen atoms bonded to Re suggest that the Re coordination polyhedra are likely to be highly disordered; however, the extent and the nature of this disorder cannot be reliably assessed from diffraction data, but could potentially be addressed by neutron total scattering studies.

Following geometry optimisation, *ab-initio* molecular dynamics simulations were performed at four temperatures to probe the oxide ion migration pathways in $\text{Bi}_{28}\text{Re}_2\text{O}_{49}$. The key conclusion is that the ability of Re to support four-, five- and six-fold coordination environments is important in this material, in that it provides a mechanism for ‘self-doping’ of the structure, i.e. the creation of vacancies in the fluorite-like Bi-O sublattice, accompanied by an increase of the average coordination number of Re. All three unique oxygen sites in this sublattice play roles in the ionic migration processes, by facilitating the O^{2-} exchange between the ReO_x groups and by contributing to the O^{2-} diffusion *via* the well-known vacancy-hopping mechanisms within the polarisable Bi-O sublattice.

This work extends the range of oxide ion conductors in which the variable cation coordination environments and the O^{2-} exchange between the highly polarisable Bi-O sublattice and a polyhedral metal-O sublattice facilitate the oxide ion mobility. The most notable example of this type of behaviour is the remarkable low-temperature oxide ion conductivity in the $\text{Bi}_{1-x}\text{V}_x\text{O}_{1.5+x}$ materials ($x = 0.087, 0.095$; $\sigma \sim 3.9 \times 10^{-2}$ S/cm at 500°C) [32] where an additional favourable structural feature is the pseudo-cubic ordered superstructure.

Other known examples include monoclinic δ -Bi₂O₃-based superstructure bismuth vanadate Bi₄₆V₈O₈₉ and bismuth molybdate Bi₂₆Mo₁₀O₆₉, which also display high oxide ion conductivity based on these concepts and mechanisms. [33],[34]; it is likely that they also play a role in the behaviour of other rhenate oxide ion conductors. [31]

Acknowledgements

Financial support was provided by the EPSRC through grant EP/F030371. JLP thanks Durham University for a PhD studentship. JDF thanks the ILL for a summer studentship. The authors thank the ILL for computational facilities and Didier Richard and Eric Pellergrini for recent developments in LAMP and nMoldyn codes.

References

- [1] R.M. Ormerod, *Chem. Soc. Rev.* **32** (2003) 17.
- [2] J.B. Goodenough, *Solid State Ionics* **94** (1997) (1-4) 17.
- [3] R. Ramamoorthy, P.K. Dutta, S.A. Akbar, *J. Mater. Sci.* **38** (2003) 4271
- [4] P. Shuk, H.D. Wiemhofer, U. Guth, W. Gopel, M. Greenblatt, *Solid State Ionics* **89** (1996) (3-4) 179.
- [5] V.V. Kharton, E.N. Naumovich, A.A. Yaremchenko, F.M.B. Marques, *J. Solid State Electrochem.* **5** (2001) (3) 160.
- [6] C.D. Ling, *J. Solid State Chem.* **148** (1999) (2) 380.
- [7] W. Zhou, *J. Solid State Chem.* **76** (1988) (2) 290.
- [8] A. Watanabe, *Solid State Ionics* **40-1** (1990) 889.
- [9] X. Kuang, M.A. Green, H. Niu, P. Zajdel, C. Dickinson, J.B. Claridge, L. Jantsky, M.J. Rosseinsky, *Nat. Mater.* **7** (2008) (6) 498.
- [10] E. Kendrick, J. Kendrick, K.S. Knight, M.S. Islam, P.R. Slater, *Nat. Mater.* **6** (2007) (11) 871.
- [11] I. R. Evans, J. S. O. Evans, J. A. K. Howard, *Chem. Mater.* **17** (2005) 4074
- [12] E. Kendrick, M.S. Islam, P.R. Slater, *J. Mater. Chem.* **17** (2007) (30) 3104.
- [13] T.E. Crumpton, J.F.W. Mosselmans, C. Greaves, *J. Mat. Chem.* **15** (2005) (1) 164.
- [14] C.H. Hervoches, C. Greaves, *J. Mat. Chem.* **20** (2010) (32) 6759.
- [15] Y.D. Li, T.P. Hutchinson, X.J. Kuang, P.R. Slater, M.R. Johnson, I.R. Evans, *Chemistry of Materials* **21** (2009) (19) 4661.
- [16] Bruker, SAINT Plus, Madison, Wisconsin.
- [17] A.C. Altomare, G.; Giacovazzo, C.; Guagliardi, A.; Burla, M.C.; Polidori, G.; Camalli, M, *Journal of Applied Crystallography* **27** (1994) 437.
- [18] P.W. Betteridge, Carruthers, J.R., Cooper, R.I., Prout, K., Watkin, D.J, *Journal of Applied Crystallography* **36** (2003) 1487.
- [19] A.A. Coelho, J.S.O. Evans, I.R. Evans, A. Kern, S. Parsons, *Powder Diffraction* **26** (2011) (4) S22.
- [20] G. Kresse, J. Furthmuller, *Comput. Mater. Sci* **6** (1996) 15.
- [21] G. Kresse, D. Joubert, *Phys. Rev. B* **59** (1999) (3) 1758.
- [22] P.E. Blochl, *Phys. Rev. B* **50** (1994) (24) 17953.
- [23] P. Hohenberg, W. Kohn, *Phys. Rev. B* **136** (1964) (3B) B864.
- [24] W. Kohn, L.J. Sham, *Phys. Rev.* **140** (1965) (4A) 1133.
- [25] J.P. Perdew, K. Burke, M. Ernzerhof, *Phys. Rev. Lett.* **77** (1996) (18) 3865.
- [26] J.P. Perdew, K. Burke, M. Ernzerhof, *Phys. Rev. Lett.* **78** (1997) (7) 1396.
- [27] M.A.M. Forgeron, R.E. Wasylishen, *Physical Chemistry Chemical Physics* **10** (2008) (4) 574.
- [28] T. Rog, K. Murzyn, K. Hinsén, G.R.J. Kneller, *J. Comput. Chem* **24** (2003) 657.
- [29] L. Holmes, L.M. Peng, I. Heinmaa, L.A. O'Dell, M.E. Smith, R.N. Vannier, C.P. Grey, *Chem. Mater.* **20** (2008) (11) 3638.
- [30] H. Muller-Buschbaum, *Zeitschrift Fur Anorganische Und Allgemeine Chemie* **633** (2007) (15) 2491.
- [31] C.H. Hervoches, C. Greaves, *Solid State Ionics* **217** (2012) 46.
- [32] X.J. Kuang, J.L. Payne, M.R. Johnson, I.R. Evans, *Angewandte Chemie International Edition* **51** (2012) 690.
- [33] X.J. Kuang, J.L. Payne, J.D. Farrell, M.R. Johnson, I.R. Evans, *Chemistry of Materials* **24** (2012) (11) 2162.
- [34] C.D. Ling, W. Müller, M.R. Johnson, D. Richard, S. Rols, J. Madge, I.R. Evans, *Chemistry of Materials* **24** (2012) (23) 4607.